Robust Nonlinear Causality Analysis of Non-Stationary Multivariate Physiological Time Series

Tim Schäck, *Student Member, IEEE,* Michael Muma, *Member, IEEE,* Mengling Feng, *Member, IEEE,*
Cuntai Guan, *Senior Member, IEEE,* Abdelhak M. Zoubir, *Fellow, IEEE*

Abstract—Goal: **An important research area in biomedical signal processing is that of quantifying the relationship between simultaneously observed time series and to reveal interactions between the signals. Since biomedical signals are potentially non-stationary and the measurements may contain outliers and artifacts, we introduce a robust time-varying generalized partial directed coherence (rTV-gPDC) function.** *Methods:* **The proposed method, which is based on a robust estimator of the time-varying autoregressive (TVAR) parameters, is capable of revealing directed interactions between signals. By definition, the rTV-gPDC only displays the linear relationships between the signals. We therefore suggest to approximate the residuals of the TVAR process, which potentially carry information about the nonlinear causality by a piece-wise linear time-varying moving-average (TVMA) model.** *Results:* **The performance of the proposed method is assessed via extensive simulations. To illustrate the method's applicability to real-world problems, it is applied to a neurophysiological study that involves intracranial pressure (ICP), arterial blood pressure (ABP), and brain tissue oxygenation level (PtiO2) measurements.** *Conclusion and Significance:* **The rTV-gPDC reveals causal patterns that are in accordance with expected cardiosudoral meachanisms and potentially provides new insights regarding traumatic brain injuries (TBI). The rTV-gPDC is not restricted to the above problem but can be useful in revealing interactions in a broad range of applications.**

*Index Terms—***Biomedical signal processing, connectivity analysis, directed coherence, Kalman filter, multivariate autoregressive modeling, time-varying autoregressive (TVAR), time-varying moving-average (TVMA), partial directed coherence (PDC), generalized partial directed coherence (gPDC), intracranial pressure (ICP), arterial blood pressure (ABP), traumatic brain injuries (TBI).**

I. INTRODUCTION

IN multivariate biomedical signal processing, an important and frequently asked question is whether the underlying time series interact and whether they are causally connected. Answering this question is of interest in many applications, for example in the case of non-invasive brain activity measurements, such as electroencephalography (EEG) or

T. Schäck, M. Muma, and A. M. Zoubir are with the Signal Processing Group, Institute of Telecommunications, Technische Universität Darmstadt, Darmstadt 64283, Germany (e-mail: schaeck@spg.tu-darmstadt.de; mmuma@spg.tu-darmstadt.de; zoubir@spg.tu-darmstadt.de).

Mengling Feng is with Saw Swee Hock School of Public Health, National University of Singapore, 12 Science Drive 2, #10-01, 117549 Singapore (e-mail: ephfm@nus.edu.sg).

Cuntai Guan is with School of Computer Science and Engineering, College of Engineering, Nanyang Technological University, 50 Nanyang Ave, 639798 Singapore (e-mail: ctguan@ntu.edu.sg).

functional magnetic resonance imaging (fMRI), where the neural connectivity is characterized [1]–[10]. Also in cardiological studies one is interested, for example, in the relation between cardiovascular and cardiorespiratory data [11]–[15].

A traditional approach to analyze the relation between multivariate biomedical signals is to use the coherence function [16], the partial coherence [17], or approaches based on time-varying extensions of the coherence function [15], [18]. However, the coherence function is not a directional measure, i.e., it does not provide the direction of the information flow. Therefore, several techniques based on linear multivariate autoregressive (MVAR) models have been proposed to quantify causality in the frequency domain. One of the most frequently applied methods is the directed transfer function (DTF), that was introduced by Kaminski and Blinowska [19] as a multivariate measure of the intensity of activity flow in brain structures. A further multivariate approach for the estimation of causality between time series is the directed coherence (DC), a terminology introduced in [20] and reviewed by Baccalá *et al.* in [2], which was first applied to analyze neural data. The partial directed coherence (PDC) and the re-examined definition of the generalized partial directed coherence (gPDC) were introduced by Baccalá *et al.* [21], [22]. The PDC is a conceptional generalization of the DC, whereas the gPDC is a natural generalized definition of the PDC. It allows to perform a multivariate analysis that is capable of detecting the interactions between two signals after removing the contribution of all the other signals. gPDC also has the advantage of being scale invariant and more accurate for short time series as compared to the PDC. Thus, the gPDC is able to distinguish between direct and indirect connections. To overcome the limitation of stationarity, Milde *et al.* [23] presented a technique to estimate high-dimensional time-variant autoregressive (TVAR) models for interaction analysis of simulated data and high-dimensional multi-trial laser-evoked brain potentials (LEP). Systematic investigations on the approach to use a Kalman filter for the estimation of the TVAR models were performed by Leistritz *et al.* [24]. A mathematical derivation of the asymptotic behaviour of the gPDC has been presented by Baccalá *et al.* [25]. Omidvarnia *et al.* [26] modified the time-varying generalized partial directed coherence (TV-gPDC) method by orthogonalization of the strictly causal multivariate autoregressive model coefficients. The generalized orthogonalized PDC (gOPDC)

minimizes the effect of mutual sources and was applied on event-related directional information flow from flash-evoked responses in neonatal EEG. All the above-mentioned multivariate measures rely on the concept of Granger causality between time series [27] and can be interpreted as frequency domain representations of this very popular concept of causality.

However, a severe challenge in estimating the parameters of MVAR models is the sensitivity of classical estimators towards artifacts or outliers in the measurements [5], [28]–[35]. The presence of artifacts or outliers was frequently reported, e.g., in fMRI [36] or ECG [35] measurements. Researchers often must exclude contaminated signal parts [5], [28], [29], [31]–[33] which can lead to a significant loss of data. Finally, since MVAR models are bound to describe linear relations between time series, they fail to detect nonlinear causalities, which have been reported for a variety of biomedical signals [37]–[39].

Our contributions are as follows: We propose a new directed coherence measure called the robust time-varying generalized partial directed coherence (rTV-gPDC). The parameters of the gPDC are estimated using a Kalman filter. In this way, the assumption of stationarity is dropped. Based on robust statistics [34], [40], [41], we introduce a computationally attractive one-step reweighting algorithm that is incorporated into the Kalman filter to handle artifacts. We adapt a method by Chowdhury [42] to approximate the often unknown nonlinear function with the help of a family of piece-wise linear functions using a TVMA model that captures causalities that cannot be explained by the TVAR model, i.e., are nonlinear. With this TVMA model, we extend the gPDC to nonlinear causality patterns to reveal nonlinear relations between multivariate time series. We evaluate our method numerically both in terms of accuracy and robustness and compare it to an existing method [43]. Further, we apply our method to clinically collected traumatic brain injury data and display the interactions between intracranial pressure (ICP), arterial blood pressure (ABP) and brain tissue oxygenation level (PtiO2) signals.

The paper is organized as follows. Section II briefly revisits some important existing methods. Section III introduces a novel time-varying frequency domain approach to assess causality between time series based on TVAR and TVMA models as an extension of the gPDC. The new approach is validated on simulated TVAR data in Section IV, whereas Section V is devoted to an application of the approach to a real clinically collected multivariate biomedical time series. Section VI discusses the approach based on the achieved results and addresses the advantages and drawbacks, before Section VII concludes the paper.

II. BACKGROUND ON MEASURING CAUSALITY IN THE FREQUENCY DOMAIN

This Section briefly reviews the TVAR model and the frequency domain causality measures including the gPDC.

A. Multivariate Autoregressive (MVAR) Model

Let $\mathbf{x}(n) = [x_1(n), x_2(n), \ldots, x_M(n)]^T$ denote an M-dimensional multivariate time series whose consecutive measurements contain information about the underlying processes. A common attempt to describe such a time series is to model the current value as a linear summation of its previous values plus an innovation term. This very popular time series model is called the MVAR model and is given by

$$\mathbf{x}(n) = \sum_{p=1}^{P} \mathbf{A}_p \mathbf{x}(n-p) + \mathbf{v}(n), \tag{1}$$

where P is the model order, $\mathbf{v}(n) = [v_1(n), v_2(n), \ldots, v_N(n)]^T$ is a white noise vector, and $\mathbf{A}_p$ are the parameters that define the time series:

$$\mathbf{A}_p = \begin{bmatrix} a_{11} & \ldots & a_{1M} \\ \vdots & \ddots & \vdots \\ a_{M1} & \ldots & a_{MM} \end{bmatrix}. \tag{2}$$

Here, a_{ij} reflects the linear relationship from channel j to channel i, where $i, j = 1, \ldots, M$.

B. Frequency Domain Causality Measures

1) Granger Causality: The economist Sir Clive W. J. Granger defined the concept of causality by exploiting the temporal relationships between time series [27], [44]. In his definition, the general idea of causality is expressed in terms of predictability: If a signal X causes a signal Y, the knowledge of the past of both X and Y should improve the prediction of the presence of Y as opposed to the knowledge of the past of Y alone.

Granger causality is based on assuming stationarity and requires a good fit of the underlying AR model to the data at hand. More recently, time-varying approaches using Granger causality have been proposed, such as in [45], [46], by incorporating TVAR models with time-dependent parameters and time-dependent estimates of the variances of the prediction errors. In addition to the time-variation, also nonlinear approaches of Granger causality have recently been published [38], [46]. A survey of Granger causality from a computational viewpoint was published by Liu and Bahadori [47].

2) Generalized Partial Directed Coherence: Based on Granger causality and MVAR models, several frequency domain based measures have been introduced to determine the directional influence in multivariate systems. One of the recently proposed methods is the PDC, introduced in the context of analyzing neural data by Baccalá in [21]. It reveals the information flow between isolated pairs of time series.

A re-examined and improved modification of the PDC was proposed by Baccalá in [22]: the generalized partial directed coherence. The gPDC aims at improving the performance under scenarios that involve severely unbalanced predictive modeling errors and it features hugely reduced variability for short time series, which is required for bootstrap-based connectivity testing approaches [22], [48], [49].

In the original definition of the gPDC, time-invariance and

stationarity of the data are required. It is based on the MVAR parameters comprised in (2), which have to be transformed into the frequency domain by

$$\bar{\mathbf{A}}(f) = I_M - \sum_{p=1}^{P} \mathbf{A}_p e^{-\mathrm{i}2\pi f p}, \qquad (3)$$

where i is the imaginary unit and f is the normalized frequency in the interval $[-0.5, 0.5]$. The gPDC [22] is defined as

$$\pi_{ij}(f) = \frac{\frac{1}{\sigma_i}\bar{A}_{ij}(f)}{\sqrt{\sum_{m=1}^{M}\frac{1}{\sigma_i^2}\bar{A}_{mj}(f)\bar{A}_{mj}^*(f)}}, \qquad (4)$$

where σ_i refers to the standard deviation of the innovations processes $v_i(n)$ and * refers to complex conjugate.

III. ROBUST TIME-VARYING GENERALIZED PARTIAL DIRECTED COHERENCE (rTV-gPDC)

This Section is dedicated to describing and analyzing our proposed methodological approach to robustly assess the linear and nonlinear causality between time series based on a new method called the robust time-varying generalized partial directed coherence (rTV-gPDC).

A. TVAR and TVMA Models for Nonlinearity Approximation

For non-stationary multivariate time series, an explicit description of the variation is necessary due to the time-dependent MVAR parameters $\mathbf{A}_p(n)$. This is realized by extending (1) to the TVAR model

$$\mathbf{x}(n) = \sum_{p=1}^{P} \mathbf{A}_p(n)\mathbf{x}(n-p) + \mathbf{v}(n), \qquad (5)$$

where $\mathbf{v}(n)$ is assumed to be a white noise process.

The TVAR model is based on linear equations; thus, it is only able to describe linear relationships between time series. However, most physiological systems are subject to more complex and nonlinear forms [50].

For example, for cerebral hemodynamics, the Blood Oxygen Level Dependent (BOLD) signal responses to stimulus temporally in a nonlinear manner, and nonlinearity has also been observed, when two identical stimuli induced close together in time produce a net response with less than twice the integrated response of a single stimulus alone [51]. It was also reported that intracranial pressure (ICP), an important indicator for secondary brain insult for traumatic brain injury (TBI) patients, is associated with the cerebral blood volume based on a nonlinear mechanism of auto-regulation [52].

If a dynamic process is not limited to linear interactions, the residuals of the linear model will not be a white noise sequence. If a specific nonlinear model is known for a given application, e.g. from medical considerations, the best option is to incorporate this information and to leverage upon this specific knowledge. In many cases, however, specific knowledge of the nonlinear function is not known, and thus a specific nonlinear modeling approach is not possible.

For this reason, we adapt the approach of [42] and approximate the unknown nonlinear function by use of a family of piece-wise linear functions. When $\mathbf{v}(n)$ is not white but colored noise, Chowdhury suggests to approximate it by

$$\mathbf{v}(n) \approx \sum_{q=1}^{Q} \mathbf{B}_q(n)\mathbf{r}(n-q) + \mathbf{r}(n). \qquad (6)$$

This approximation of the unknown nonlinear function is obtained by extending the TVAR model in (5) by a stochastic TVMA term (6) to

$$\mathbf{x}(n) = \sum_{p=1}^{P} \mathbf{A}_p(n)\mathbf{x}(n-p) + \sum_{q=1}^{Q} \mathbf{B}_q(n)\mathbf{r}(n-q) + \mathbf{r}(n) \quad (7)$$

with $n = 1, \ldots, N$ and Q being the order of the MA part. Here, $\mathbf{B}_q(n)$ is the time-varying $M \times M$ parameter matrix that weights past values of $\mathbf{r}(n)$. If $\mathbf{v}(n)$ contains a structure which could not be incorporated into the linear TVAR model, the partly nonlinear relationship is approximated by the TVMA term. Analogous to (2), we define the time-varying residual parameter matrix $\mathbf{B}_q(n)$ as follows:

$$\mathbf{B}_q(n) = \begin{bmatrix} b_{11}(n) & \ldots & b_{1M}(n) \\ \vdots & \ddots & \vdots \\ b_{M1}(n) & \ldots & b_{MM}(n) \end{bmatrix}. \qquad (8)$$

The time-varying residual parameter matrix $\mathbf{B}_q(n)$ and the corresponding nonlinear extension of the TV-gPDC in (11) are only greater than zero if the interactions of the signals are nonlinear, as all linear interactions are captured by the TVAR model and the corresponding linear TV-gPDC in (9).

B. Linear and Nonlinear Causality Analysis

A time-varying version of the gPDC can be obtained by incorporating the TVAR model from (5) with the corresponding time-dependent parameter matrix $\mathbf{A}_p(n)$. A time-varying gPDC (TV-gPDC) is then defined as

$$\pi_{ij}^A(n, f) = \frac{\frac{1}{\sigma_i(n)}\bar{A}_{ij}(n, f)}{\sqrt{\sum_{m=1}^{M}\frac{1}{\sigma_i^2(n)}\bar{A}_{mj}(n, f)\bar{A}_{mj}^*(n, f)}}. \qquad (9)$$

To further incorporate the nonlinear connectivity, the additional time-varying residual parameter matrix $\mathbf{B}_j(n)$ is transformed analogously to the linear term by

$$\bar{\mathbf{B}}(n, f) = \sum_{q=1}^{Q} \mathbf{B}_q(n)e^{-\mathrm{i}2\pi f q}. \qquad (10)$$

We thus propose the nonlinear extension of the TV-gPDC as

$$\pi_{ij}^B(n, f) = \frac{\frac{1}{\sigma_i(n)}\bar{B}_{ij}(n, f)}{\sqrt{\sum_{m=1}^{M}\frac{1}{\sigma_i^2(n)}\bar{B}_{mj}(n, f)\bar{B}_{mj}^*(n, f)}} \qquad (11)$$

by integrating $\bar{\mathbf{B}}(n, f)$ from (11) into the definition of the TV-gPDC.

The separation between linear and nonlinear causalities helps in displaying nonlinear interactions by use of approximation in situations where no specific nonlinear model exists and in detecting moments when the causality becomes strongly or almost purely nonlinear. However, while the MA part reflects the presence of nonlinear causalities, it is likely quantified, if only partly, also by the linear AR part of the model.

C. Robust Estimation of TVAR and TVMA Model Parameters

The estimation of the time-varying parameter matrices $\mathbf{A}_p(n)$ and $\mathbf{B}_q(n)$ can be performed in different ways. One way is to evaluate the signals within moving short-time windows and to assume local stationarity. Another approach is to estimate the time-varying parameters with adaptive filters, such as the RLS algorithm [53], the LMS algorithm [28] or the Kalman filter [23]. One advantage of the latter approach is the absence of the local stationarity assumption.

Another advantage is the possibility to incorporate statistically robust estimators, e.g., the robustly filtered τ-, M- or S-estimators [34], [41] into the the adaptive filter algorithms. As biomedical signals are often contaminated by artifacts or outlying values, it is advisable to estimate TVAR and TVMA model parameters robustly. However, advanced robust methods for dependent data are not always applicable because of their high computational complexity [34], [41]. Therefore, we introduce a computationally light and robust one-step reweighting algorithm in this paper.

1) Transition to the State Space Model: Since the Kalman filter estimates the state of a state space model, the TVAR and TVMA models must be defined in the state space [54]. This is achieved by using the following notation

$$\mathbf{a}(n) = \text{vec}\left([\mathbf{A}_1(n), \mathbf{A}_2(n)\ldots,\mathbf{A}_P(n)]^T\right) \quad (12)$$
$$\mathbf{b}(n) = \text{vec}\left([\mathbf{B}_1(n), \mathbf{B}_2(n)\ldots,\mathbf{B}_Q(n)]^T\right) \quad (13)$$

$$\boldsymbol{\theta}(n) = \begin{bmatrix} \mathbf{a}(n) \\ \mathbf{b}(n) \end{bmatrix}, \quad (14)$$

where $\mathbf{a}(n)$ is the $PM^2 \times 1$ AR parameter vector, $\mathbf{b}(n)$ is the $QM^2 \times 1$ MA parameter vector, and $\boldsymbol{\theta}(n)$, as defined in (14), is the unknown parameter vector of dimension $(P+Q)M^2 \times 1$.

The prediction error

$$\hat{\mathbf{r}}(n) = \mathbf{x}(n) - \hat{\mathbf{x}}(n|n-1) \quad (15)$$

is defined by the residual of the estimation process from previous time-steps, where $\hat{\mathbf{x}}(n|n-1)$ is the *a priori* estimate of $\mathbf{x}(n)$, given information up to the previous time step.

The TVAR and TVMA models can then be represented in the state space by making the following definitions:

$$\tilde{\mathbf{X}}(n) = [\mathbf{x}^T(n-1), \mathbf{x}^T(n-2),\ldots,\mathbf{x}^T(n-P)] \quad (16)$$
$$\tilde{\mathbf{R}}(n) = [\hat{\mathbf{r}}^T(n-1), \hat{\mathbf{r}}^T(n-2),\ldots,\hat{\mathbf{r}}^T(n-Q)] \quad (17)$$

$$\mathbf{C}(n) = \mathbf{I}_M \otimes \tilde{\mathbf{X}}^T(n) \quad (18)$$
$$\mathbf{D}(n) = \mathbf{I}_M \otimes \tilde{\mathbf{R}}^T(n) \quad (19)$$

$$\boldsymbol{\Phi}(n) = \begin{bmatrix} \mathbf{C}(n) \\ \mathbf{D}(n) \end{bmatrix} \quad (20)$$

Here, $\tilde{\mathbf{X}}(n)$ contains the P previous measurements, $\tilde{\mathbf{R}}(n)$ represents the Q previous residuals defined in (15), $\otimes$ represents the Kronecker product, and $\boldsymbol{\Phi}(n)$ is the $(P+Q)M^2 \times M$ matrix representing previous measurements $\mathbf{C}(n)$ and residuals $\mathbf{D}(n)$.

When estimating the TVAR and TVMA model parameters, the observation is given by $\mathbf{x}(n)$ and $\boldsymbol{\theta}(n)$ is the unknown parameter vector that is sought for. Thus, the system equation of the Kalman filter is given by

$$\boldsymbol{\theta}(n) = \boldsymbol{\theta}(n-1) + \mathbf{w}(n), \quad (21)$$

where $\boldsymbol{\theta}(n)$ and $\boldsymbol{\theta}(n-1)$ are the current and previous state, respectively, and $\mathbf{w}(n)$ is the noise term with $\mathbf{w}(n) \sim \mathcal{N}(0, \mathbf{Q})$.

As it is not possible to measure the true state $\boldsymbol{\theta}(n)$ itself, but an observation $\mathbf{x}(n)$, the measurement equation is given by

$$\mathbf{x}(n) = \boldsymbol{\Phi}^T(n)\boldsymbol{\theta}(n) + \boldsymbol{\xi}(n), \quad (22)$$

where the measurement noise $\boldsymbol{\xi}(n)$ is distributed as $\mathcal{N}(0, \mathbf{R}(\mathbf{n}))$, i.e. in this work, we assume that the covariance of the measurement noise $\mathbf{R}(n)$ is time-varying.

2) The Kalman Filter Implementation: The Kalman filter consists of a prediction and a correction step. The one-step ahead prediction of the parameter vector $\hat{\boldsymbol{\theta}}(n|n-1)$ and of the state covariance matrix $\hat{\mathbf{P}}(n|n-1)$ are given by

$$\hat{\boldsymbol{\theta}}(n|n-1) = \hat{\boldsymbol{\theta}}(n-1) \quad (23)$$
$$\hat{\mathbf{P}}(n|n-1) = \hat{\mathbf{P}}(n-1) + \hat{\mathbf{Q}}, \quad (24)$$

where $\hat{\mathbf{Q}}$ is the estimate of the system noise covariance matrix, defined as $\hat{\mathbf{Q}} = \lambda \mathbf{I}_L$. The state covariance matrix $\hat{\mathbf{P}}(0|0)$ is initialized with the $PM^2 \times PM^2$ identity matrix.

The correction step is performed as follows:

$$\mathbf{G}(n) = \hat{\mathbf{P}}(n|n-1)\boldsymbol{\Phi}(n)\left[\boldsymbol{\Phi}^T(n)\hat{\mathbf{P}}(n|n-1)\boldsymbol{\Phi}(n)\ldots \right.$$
$$\left. + \mathbf{R}(n)\right]^{-1} \quad (25)$$

$$\hat{\boldsymbol{\theta}}(n) = \hat{\boldsymbol{\theta}}(n|n-1) + \mathbf{G}(n)\hat{\mathbf{r}}(n) \quad (26)$$
$$\hat{\mathbf{P}}(n) = \left[\mathbf{I}_{(P+Q)M^2} - \mathbf{G}(n)\boldsymbol{\Phi}^T(n)\right]\hat{\mathbf{P}}(n|n-1). \quad (27)$$

First, the $(P+Q)M^2 \times M$-dimensional gain $\mathbf{G}(n)$ needs to be computed. The measurement noise covariance matrix $\mathbf{R}(n)$ is given by

$$\mathbf{R}(n) = (1-\lambda)\mathbf{R}(n-1) + \lambda\hat{\mathbf{r}}(n)\hat{\mathbf{r}}(n)^T \quad (28)$$

with $\mathbf{R}_0 = \mathbf{I}_M$ and with $\hat{\mathbf{r}}(n)$ being the prediction error that is defined as

$$\hat{\mathbf{r}}(n) \quad = \quad \mathbf{x}(n) - \hat{\mathbf{x}}(n|n-1) \quad (29)$$
$$\mathbf{x}(n) - \boldsymbol{\Phi}^T(n)\hat{\boldsymbol{\theta}}(n|n-1). \quad (30)$$

λ is the update coefficient, which is a constant that has to be set *a priori*. The higher the value of λ, the quicker the model will adapt to changes, i.e. the more influence is given to the current prediction error.

The second equation of the correction step (26) yields an *a*

posteriori estimate of the model parameters $\hat{\boldsymbol{\theta}}(n)$ by weighting the *a priori* error. The *a posteriori* state covariance matrix $\hat{\mathbf{P}}(n)$ is given by (27).

3) Proposed Robust Algorithm: In order to reduce the influence of outliers, we develop a one-step reweighting algorithm, which we incorporate into the Kalman filter. In physiological measurements, the major concern are additive outliers in the observations that are caused by subject motion and constitute an external non-Gaussian contamination process. As can be deduced from the state space model, a single outlier can contaminate multiple prediction errors in the parameter estimation algorithm of the standard Kalman filter. The procedure of the proposed robust algorithm is shown in Fig. 1. For each univariate time series and each time step n, the algorithm proceeds as follows:

Let $\tilde{\mathbf{x}}_m(n)$ be defined by

$$\tilde{\mathbf{x}}_m(n) = [x_m(n - \frac{L}{2}), \dots, x_m(n), \dots, x_m(n + \frac{L}{2})]. \quad (31)$$

Then, we robustly estimate the mean of $\tilde{\mathbf{x}}_m(n)$ by

$$\hat{\mu}_{\text{rob},n}(\tilde{\mathbf{x}}_m(n)) = \text{median}\left(\tilde{\mathbf{x}}_m(n)\right), \quad (32)$$

where L is an even integer. The normalized median absolute deviation (MAD) is used to robustly estimate the standard deviation of the univariate prediction error $\tilde{\mathbf{r}}_m(n)$

$$\hat{\sigma}_{\text{mad},n}(\tilde{\mathbf{r}}_m(n)) = 1.4826 \cdot \text{median}\left(|\tilde{\mathbf{r}}_m(n) - \text{median}(\tilde{\mathbf{r}}_m(n))|\right) \quad (33)$$

with

$$\tilde{\mathbf{r}}_m(n) = [\hat{r}_m(n - L), \dots, \hat{r}_m(n)]. \quad (34)$$

The constant in (33) provides consistency with respect to a Gaussian distribution [34], [41]. Both the robust mean of the time series and the robust standard deviation of the prediction error are time-varying. Next, we determine a threshold

$$c_i(n) = k \cdot \hat{\sigma}_{\text{mad},n}(\tilde{\mathbf{r}}_m(n)), \quad (35)$$

where the tuning constant k depends on the chosen weighting function and is set to $k = 4.685$ and $k = 1.345$ for Huber's weighting function and bisquare weighting function, respectively [41].

Based on (35), if the current sample $x_m(n)$ does not exceed the threshold $c_i(n)$ around the robust time-varying mean (32), it is assumed to be noncorrupted, and it is passed to the Kalman filter. If

$$|x_m(n) - \hat{x}_m(n|n - 1)| > c_m(n), \quad (36)$$

the sample $x_m(n)$ is assumed to be corrupted. Therefore, a weight

$$w_{x_m(n)}(n) = W(y(n) - \hat{\mu}_{\text{rob},n}(\tilde{\mathbf{y}}(n))) \quad (37)$$

is calculated using either Huber's or the bisquare type weighting function.

After having determined $w(n)$, the outlier-cleaned observation at time instant n is computed by

$$x^*(n) = w(n)x(n) + (1 - w(n))\hat{x}(n). \quad (38)$$

It is then concatenated with the previous univariate samples to form the outlier-cleaned current multivariate observation

$\mathbf{x}^*(n)$. With $x^*(n)$, the Kalman filter can calculate a robustified prediction error

$$\bar{\mathbf{r}}(n) = \mathbf{x}^*(n) - \boldsymbol{\Phi}^T(n)\hat{\boldsymbol{\theta}}(n|n - 1). \quad (39)$$

It is important to note that also (16), (18), and (20) need to be updated after each calculation of the cleaned time series value $\mathbf{x}^*(n)$ if (36) is true. If (36) does not hold for any of the samples, the proposed robust algorithm reduces to the classical Kalman filter.

IV. METHOD VALIDATION

In this Section, a validation of the proposed algorithms is presented. The first simulation evaluates the TVAR parameter estimation by investigating its robustness against outliers and its computational cost, whereas the second simulation is performed to evaluate the proposed nonlinear causality measure.

A. Simulation Models

In the first simulation, we consider a second order 3-dimensional MVAR process, which consists of two damped stochastically driven oscillators x_2 and x_3 as well as of a stochastically driven relaxator x_1. This simulation has previously been used in [43] and [55] to evaluate time-varying directed interactions in multivariate neural data, and was chosen in order to be comparable with preceding approaches.

The model of the first simulation is given by

$$x_1(n) = 0.59x_1(n - 1) - 0.20x_1(n - 2) + \dots$$
$$b(n)x_2(n - 1) + c(n)x_3(n - 1) + r_1(n) \quad (40)$$
$$x_2(n) = 1.58x_2(n - 1) - 0.96x_2(n - 2) + r_2(n) \quad (41)$$
$$x_3(n) = 0.60x_3(n - 1) - 0.91x_3(n - 2) + r_3(n) \quad (42)$$

with $N = 5,000$ and time-varying parameters $b(n)$ and $c(n)$. The parameter $b(n)$ is a decaying oscillating function of n and describes the influence of $x_2(n)$ on $x_1(n)$. The influence of $x_3(n)$ on $x_1(n)$ is modeled by parameter $c(n)$, which is a triangular function between 0 and 1. The signal model is driven by zero-mean unit variance Gaussian white noise process $r_i(n)$.

In the second simulation, we consider a second order 3-dimensional signal where the model contains nonlinear causality

$$x_1(n) = 0.59x_1(n - 1) - 0.20x_1(n - 2) + \dots$$
$$\sqrt{|x_3(n - 1)^3|} + r_1(n) \quad (43)$$
$$x_2(n) = 1.58x_2(n - 1) - 0.96x_2(n - 2) + r_2(n) \quad (44)$$
$$x_3(n) = 0.60x_3(n - 1) - 0.91x_3(n - 2) + \dots$$
$$x_2(n - 1) + r_3(n). \quad (45)$$

Again, the signals are driven by standard normal white noise processes $r_i(n), i = 1, 2, 3$. Here, $x_1(n)$ is nonlinearly influenced by $x_3(n)$ and $x_3(n)$ is linearly influenced by $x_2(n)$. The causality patterns are expected to express the relations between $x_1(n)$ and $x_2(n)$ and $x_3(n)$, respectively.
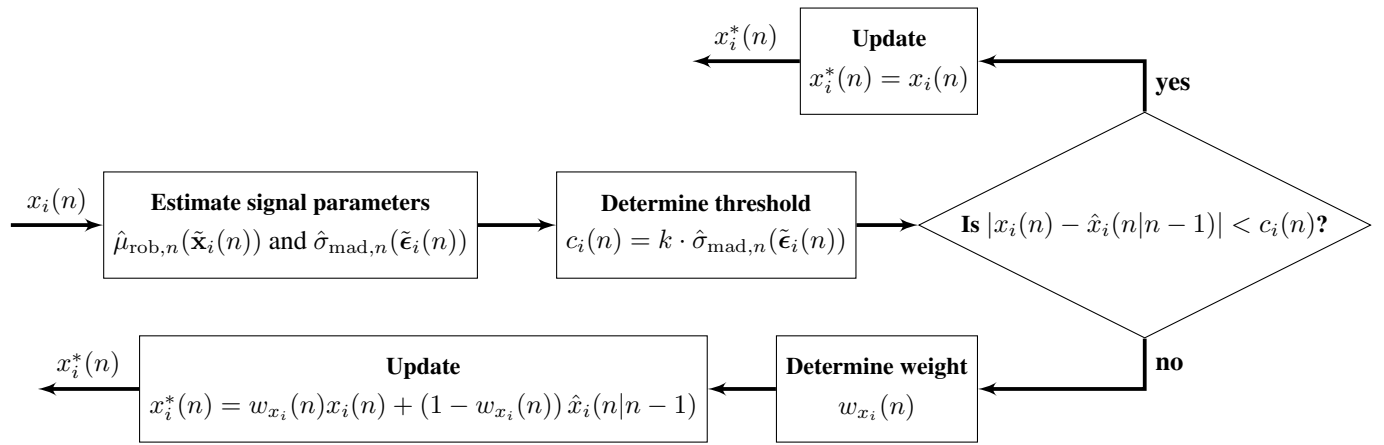
Fig. 1. The procedure of the proposed robust algorithm

B. Setup of Simulation Evaluation

1) Parameter Estimation: In most of the publications on causality analysis, only the resulting connectivity patterns are evaluated in simulations. However, in this work, we first evaluate the TVAR parameter estimation in terms of its accuracy w.r.t. the original parameters. For this purpose, we calculate the mean square error (MSE) of the estimated parameter coefficients $\hat{a}_{ij}(\lambda, n)$ given as

$$\text{MSE}(\lambda) = \frac{1}{NM^2} \sum_{n=1}^{N} \sum_{i=1}^{M} \sum_{j=1}^{M} \left(a_{ij}(\lambda, n) - \hat{a}_{ij}(\lambda, n) \right)^2 \quad (46)$$

as a function of the update coefficient λ to gain a comparable quality criterion.

In order to compare the result to existing methods, the dual extended Kalman filter (DEKF) from [43] has been evaluated with the same simulation model and has also been iterated with different values of the update coefficient.

2) Causality Analysis: To verify the correctness of the causality coherence analysis, the causal coherence patterns of the first simulation model are analyzed. As the first simulation model is constructed such that only $x_1(n)$ is driven by $x_2(n)$ and $x_3(n)$, only two connectivity patterns should have values that differ from zero.

3) Robustness Against Outliers: A very important problem in estimating the TVAR parameters is the sensitivity towards artifacts or outliers in the data. Since biomedical signals are frequently contaminated by artifacts or outliers [5], [28]–[35], researchers often exclude contaminated measurements which results in significant data loss.

To evaluate the results concerning robustness against outliers, we use a measure of robust statistics, i.e., the the maximum bias curve (MBC) [34]. The MBC reflects maximally possible asymptotic bias induced by a specific amount of contamination. The classical definition of the MBC [41] cannot be straight forwardly applied to the TVARMA model, since the non-stationarity of the data must be taken into account, which yields

$$\text{MBC}(\nu, \theta(n)) = \max\left\{ |b_{\hat{\theta}(n)}(F, \theta(n))| : F \in \mathcal{F}_{\nu,\theta(n)}, \forall n \right\} \quad (49)$$

where $\mathcal{F}_{\nu,\theta(n)} = \{(1-\nu)F_{\theta(n)} + \nu G\}$ is an ν-neighborhood of distributions around the nominal distribution $F_{\theta(n)}$ with G being an arbitrary contaminating distribution. In the non-stationary setting, the $\text{MBC}(\nu, \theta(n))$ thus also captures transient instability of the filter due to changes in the data.

In practice, even for simple (stationary lower order) AR models, the MBC cannot be computed analytically [41]. We therefore approximate the MBC at every time-step n by a Monte Carlo procedure analogous to [41], p. 305–306. The empirical MBC which we obtain displays the worst-case bias over all Monte Carlo runs and time instances. By choosing a very large variance in the outlier generating process and choosing the worst case over 1000 Monte Carlo experiments, for all time-instances, the empirical MBC as closely as possible retains the meaning of the definition given in Equation (49).

The outlier model consists of additive independently and randomly placed outliers over the course of the signal $x(n)$, where each outlier has a random sign and a value in the range of i) $\pm(3, 10) \times \hat{\sigma}_{\text{mad}}$ and ii) $\pm 10\,000 \times \hat{\sigma}_{\text{mad}}$. In model i), outliers exhibit values in a very close sigma range to the true data values, whereas model ii) simulates values heavily deviating from the bulk of the data to analyze the worst case performance. The outliers are only introduced to $x_1(n)$ in the first simulation, $x_2(n)$ and $x_3(n)$ are kept clean.

4) Computational Time: Another property of interest is the computational time of the parameter estimation as well as of the causality measure calculation. For the parameter estimation, the main critical factors are the determined AR and MA model orders P and Q, respectively, and the number of time series M. The number of parameters to be estimated is $(P + Q)M^2$.

Moreover, for the causality measure calculation, the frequency resolution is an additional parameter, which needs to be considered. The orders and signal dimension are not only crucial for the parameter estimation but also for the causality measure calculations. Extensive simulations have been performed for various settings and results are shown
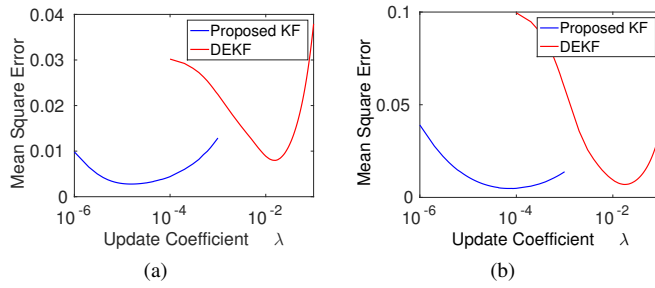
Fig. 2. Averaged MSE of (a) the parameter matrix $\mathbf{A}(n)$ and of (b) the time-varying parameter $b(n)$ and $c(n)$ as a function of the update coefficient λ. Averaged MSE for $b(n)$ and $c(n)$ are calculated as given in (46). Optimal values of λ are obtained for (a) $\lambda_{\mathrm{opt,KF}} = 1.5 \cdot 10^{-5}$ and $\lambda_{\mathrm{opt,DEKF}} = 1.5 \cdot 10^{-2}$ and for (b) $\lambda_{\mathrm{opt,KF}} = 8.3 \cdot 10^{-5}$ and $\lambda_{\mathrm{opt,DEKF}} = 1.8 \cdot 10^{-2}$.

Fig. 3. Parameter estimation of (a) parameter $b(n)$ and (b) parameter $c(n)$ with the optimal update coefficient.

depending on all of the above mentioned parameters.

5) Nonlinearity: For the nonlinearity validation, we consider the second simulation model, which incorporates linear and nonlinear causalities. $x_1(n)$ is nonlinearly influenced by $x_3(n)$, and $x_2(n)$ linearly influences $x_3(n)$. The causality patterns are expected to express the relations between $x_1(n)$ and $x_2(n)$ and $x_3(n)$, respectively. The causality of $x_2(n)$ on $x_3(n)$ is only expected to show up in the linear causality patterns, whereas the nonlinear causality of $x_3(n)$ on $x_1(n)$ can also result in some residual linear patterns.

For this setting, $N = 5,000$ and 256 frequency bins are used for a normalized frequency range $[0, 0.5]$, and the proposed robust Kalman filter is evaluated for $\lambda = 1.8 \cdot 10^{-8}$, $P = 2$ and $Q = 4$.

C. Simulation Results

1) Parameter Estimation: Fig. 2a shows the averaged MSE of the parameter matrix $\mathbf{A}(n)$ using the proposed robust Kalman filter (KF) and the DEKF [43], calculated as given in (46). The averaged MSE of the estimators with respect to the true time-varying parameters $b(n)$ and $c(n)$ is shown in Fig. 2b, likewise for the proposed Kalman filter and the DEKF. For the whole parameter matrix $\mathbf{A}(n)$, the optimal update coefficient λ for the proposed robust Kalman filter algorithm is empirically determined as $\lambda_{\mathrm{opt,KF}} = 1.5 \cdot 10^{-5}$, whereas the optimal update coefficient for the DEKF algorithm equals $\lambda_{\mathrm{opt,DEKF}} = 1.5 \cdot 10^{-2}$. As it can be observed, the proposed algorithm obtains lower averaged MSE values at the optimal update coefficient value compared to the DEKF algorithm.

Fig. 3 shows the estimation of the TVAR parameters $b(n)$ and $c(n)$ for the optimal update coefficient value over time, for the proposed Kalman filter as well as for the DEKF. The accuracy is very similar, and the estimate of the proposed robust Kalman filter is slightly closer to the true parameter value.

2) Causality Analysis: The result of the causality analysis for the first simulation model is shown in Fig. 4 and successfully reflects the time-varying partial connectivity from channel 2 to channel 1 and from channel 3 to channel 1. The causality from channel i to channel j is indicated by a directional arrow, such as, $x_i \rightarrow x_j$, $i, j = 1, 2, 3$. The frequency resolution is set to $\Delta f = 1/128$ on the normalized frequency
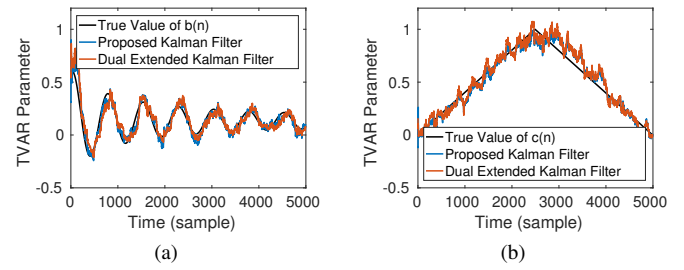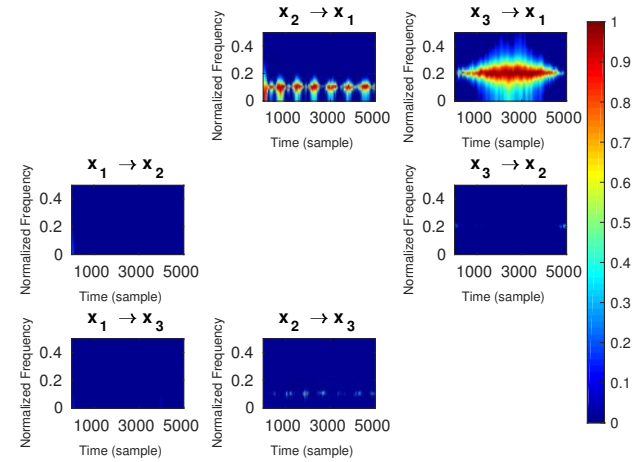

Fig. 4. Time-varying generalized partial directed coherence of the first simulation model using the proposed robust Kalman filter. The y-axis represents the normalized frequency and the x-axis represents time direction expressed in data samples.

range from 0 to 0.5. To evaluate statistical significance, we have applied the surrogate data method by [56] with 1,000 realizations and determined the 95 % significance level of the empirical distribution under the null-hypothesis of non-causality to be 0.06.

3) Robustness: The simulations regarding the robustness of the estimators are again conducted for the proposed robust Kalman filter as well as for the DEKF. Both algorithms are evaluated using the first simulation model and outlier models i) and ii). The simulations are performed using 1,000 Monte Carlo experiments for each scenario. Both estimator's bias characteristics are depicted in Fig. 5. Figures 5a and 5b are obtained using outlier model i) and Fig. 5c and 5d show the results using outlier model ii).

For a contamination with outliers having a small variance, as shown in Fig. 5a and Fig. 5b, both the proposed robust Kalman filter and the DEKF achieve reasonable results and the proposed method outperforms the DEKF both on average and in the worst case. A huge performance gain is visible in Fig. 5c compared to Fig. 5d, i.e., when the signal is contaminated by large-valued outliers. In Fig. 5d, the DEKF immediately breaks down after contaminating the signal with only 1 % of outliers. The proposed robust Kalman filter has a limited bias even up to 30 percent of gross outlier contamination.

4) Computational Time: Average computation times are obtained by using the first simulation model, varying model
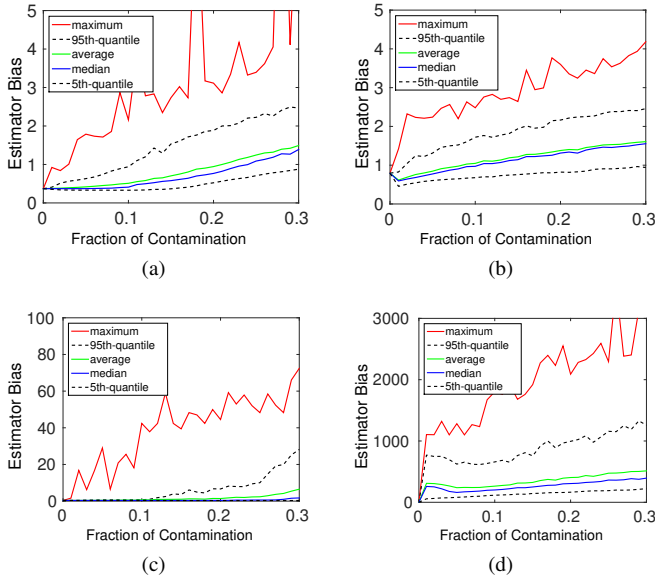
Fig. 5. Estimator bias curves showing the maximum, average, and median bias as well as its 95th- and 5th-quantile for (a) the proposed robust Kalman filter with outlier model i), (b) the proposed robust Kalman filter with outlier model ii), (c) the dual extended Kalman filter with outlier model i), and (d) the dual extended Kalman filter with outlier model ii).
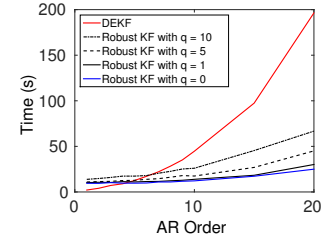

Fig. 6. Computational times of the parameter estimation depending on the AR model order P and the order Q of the MA term using the proposed robust Kalman filter algorithm and the DEKF algorithm. The simulations are evaluated with random TVAR and TVMA model parameter values, $M = 2$ dimensions and $N = 5,000$ samples.
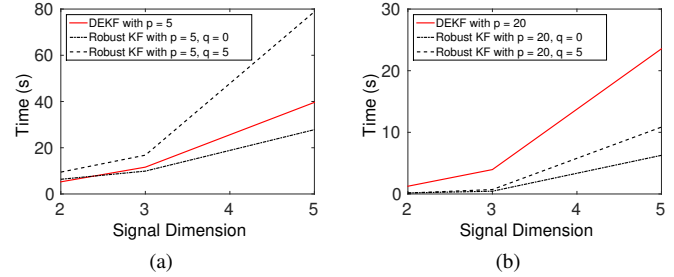

Fig. 7. Computational time of the parameter estimation depending on the signal dimensions M using the proposed robust Kalman filter and the DEKF. The simulations are evaluated with random TVAR and TVMA model parameter values, $N = 5,000$ samples and (a) AR model order $P = 5$ and (b) AR model order $P = 20$. Be aware of the change in y-axes labels from seconds to minutes.
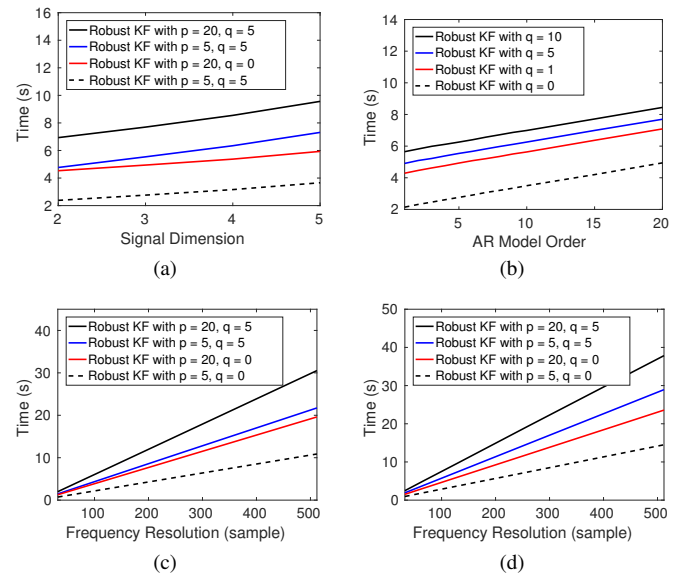

Fig. 8. Computational time of the analysis depending on (a) the signal dimension M, (b) the AR model order P, (c) the frequency resolution with signal dimension $M = 2$, and (d) the frequency resolution with signal dimension $M = 5$. The simulations are evaluated with random model parameter values and $N = 1,000$ samples.

orders $P = 1 : 10, 15, 20$ and $Q = 0, 1, 5, 10$, and multivariate signals with a maximum of 10 dimensions. All results are averaged over 100 Monte Carlo runs. The computational time of the parameter estimation using the proposed robust Kalman filter is compared with the one of the DEKF. All the computational time estimations have been performed using a MATLAB R2012a environment on a PC equipped with Intel Core i5-760 processor (2.80 GHz) and 8 GB RAM.

Fig. 6 shows the computational times for the proposed Kalman filter as well as for the DEKF. It can be seen that the DEKF is only faster for very low orders up to $P = 4$, but the computational time grows faster with increasing order. At an order of 20, for example, the proposed algorithm is almost 8 times faster than the DEKF approach, if the MA order is set to zero. But even with an MA order $Q = 5$, the proposed algorithm is still more than 4 times faster compared to the DEKF approach.

In Fig. 7, the computational times depending on the signal dimensions are depicted. Fig. 7a shows the times for fixed AR model order $P = 5$ for the proposed robust Kalman filter with MA model order $Q = 0$ and $Q = 5$ as well as, for comparison, the times for the DEKF. The AR model order is fixed to $P = 20$ in Fig. 7a.

According to Figs. 6 and 7, these plots reveal the superiority of the proposed method in terms of computational cost in the case of higher signal dimensions. After having estimated the required model parameters, the rTV-gPDC calculation is performed. The computational times of the rTV-gPDC calculation mainly depend on the frequency resolution and on the size of the estimated parameter matrices. The simulations are based on a fixed sample length $N = 1,000$ and the frequency resolution as well as the estimated parameters are varied.

The results are illustrated in Fig. 8. Both the model orders P

and Q, varied in Fig. 8b, and the frequency resolution, shown in Fig. 8c and Fig. 8d, approximately linearly depend on the computation time, whereas in Fig. 8a the computational time grows faster for higher signal dimensions M. This is due to the quadratic impact of M to the parameter order $(P+Q)M^2$.
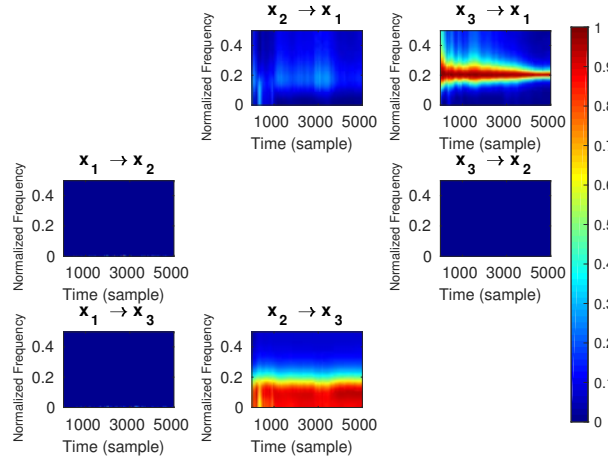
Fig. 9. Linear time-varying generalized partial directed coherence of the second simulation model using the proposed robust Kalman filter. The y-axes represent the normalized frequency and the x-axes represent time direction expressed in data samples.
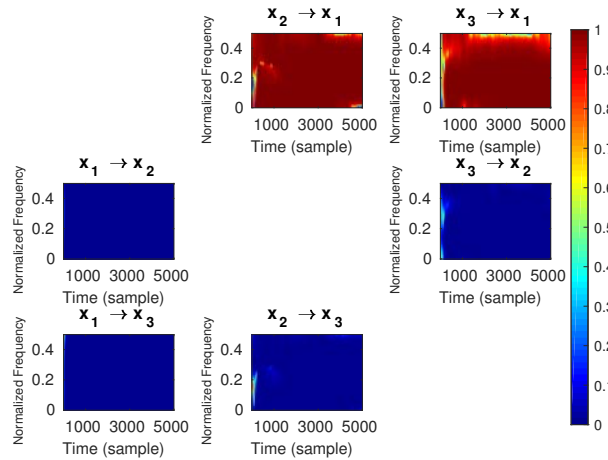

Fig. 10. Nonlinear time-varying generalized partial directed coherence of the second simulation model using the proposed robust Kalman filter. The y-axes represent the normalized frequency and the x-axes represent time direction expressed in data samples.

5) Nonlinearity: The causal patterns of the causality analysis are shown in Fig. 9 and Fig. 10 for the linear and nonlinear causality, respectively. As expected, the linear rTV-gPDC shows influence in the case of nonlinear causality from $x_3(n)$ to $x_1(n)$, and in case of linear causality from $x_2(n)$ to $x_3(n)$, whereas its nonlinear extension only recognizes the nonlinear relation between $x_3(n)$ to $x_1(n)$ and the indirect nonlinear influence of $x_2(n)$ to $x_1(n)$ over $x_3(n)$.

V. APPLICATION TO BIOMEDICAL TIME SERIES OF TRAUMATIC BRAIN INJURY PATIENTS

This Section describes the application of the proposed method to a multivariate biological time series of traumatic brain injury (TBI) patients.

For TBI patients, continuous monitoring of physiological signals, such as ICP, mean arterial blood pressure (MAP) or brain tissue oxygen level (PtiO2), has become a golden standard in neuro-intensive care units (ICU). As the primary insult, the initial mechanical damage, cannot be therapeutically reversed, the main target for TBI patient management is to limit or to prevent secondary insults through continuous physiological signal monitoring.

Cerebrovascular autoregulation is one of the important mechanisms to sustain adequate cerebral blood flow [57], and impairment of this mechanism indicates an increased risk to secondary brain damage and mortality [58]. Cerebrovascular autoregulation is most commonly assessed based on the pressure-reactivity index (PRx), which is defined as a sliding window linear correlation between the ICP and ABP. [59]. However, as reported in [52], [60], the cerebrovascular autoregulation is governed by a nonlinear mechanism. Thus, capturing the nonlinear association between ICP and MAP can offer a more complete understanding of the autoregulation process.

However, since the ICP, MAP and PtiO2 signals were collected in actual ICU environments and the sensors are sensitive to patient movements and bed angles, they are often contaminated by noise and artifacts [61], [62], see e.g. Fig. 12.

The medical data have been recorded at the Neuro-ICU of the National Neuroscience Institute, Singapore. 10 patients were considered for the analysis. From a total number of twelve different measured signals, three signals have been extracted for further analysis: ICP, MAP, and brain tissue oxygenation level (PtiO2). The pressures as well as the PtiO2 are measured in mmHG. The sampling frequency of all data is $f_s = 0.1$ Hz and no additional denoising or preprocessing has been performed except for subtracting the mean. None of the patients demongraphic nor personal information were used in this study. The proposed robust Kalman filter is applied to quantify the linear and nonlinear information transfer among ICP, MAP and PtiO2 for TBI patients.

The choice of the optimal model parameters for real signals is not straightforward as in the case of simulated data. Since we do not know the true underlying TVAR and TVMA model orders, we resort to model order selection [63]. In our case, we use an Akaike type criterion, whose minimum provides a model fit that trades off model error and complexity. As we deal with multivariate signals and need to optimize parameters of a time-varying system, only an average optimal choice can be found. The criterion is given by

$$\mathrm{AIC}(P, Q, \lambda) = \log(\det(\hat{\boldsymbol{\sigma}}_{\bar{\mathbf{r}}}^2(\lambda))) + \frac{2(P+Q)M^2}{N}, \quad (47)$$

where $\hat{\boldsymbol{\sigma}}_{\bar{\mathbf{r}}}^2$ is an estimate of the covariance matrix of the revised prediction error $\bar{\mathbf{r}}(n)$.

The optimal model orders and optimal update coefficient were estimated using (47). All available physiological signals have been used for the model order selection. As it is based on the covariance matrix of the revised prediction error $\bar{\mathbf{r}}(n)$, the criterion is robust against artifacts and there was no need to exclude certain parts of the signals. As an outcome, the
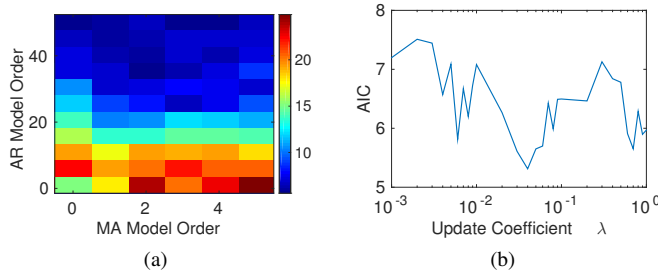
(a)   (b)

Fig. 11. Model order selection based on Akaike criterion (47) and evaluated for (a) the AR and MA model orders P and Q, and (b) for the update coefficient λ. The optimal AR model order is determined to be $P_{\mathrm{opt}} = 35$ and the optimal MA model order is found to be $Q_{\mathrm{opt}} = 2$, where the Akaike criterion takes its minimum value. The optimal coefficient value is $\lambda_{\mathrm{opt}} = 0.04$.
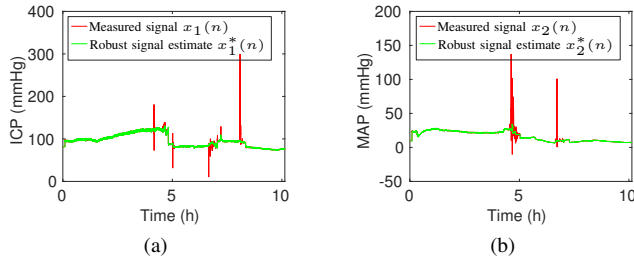

(a)   (b)

Fig. 12. An example of the robust signal estimates and the measured signals for (a) ICP and (b) MAP. Both measured signals exhibit multiple artifacts, of which the sharp spikes are commonly caused by movements of patients or sensors.

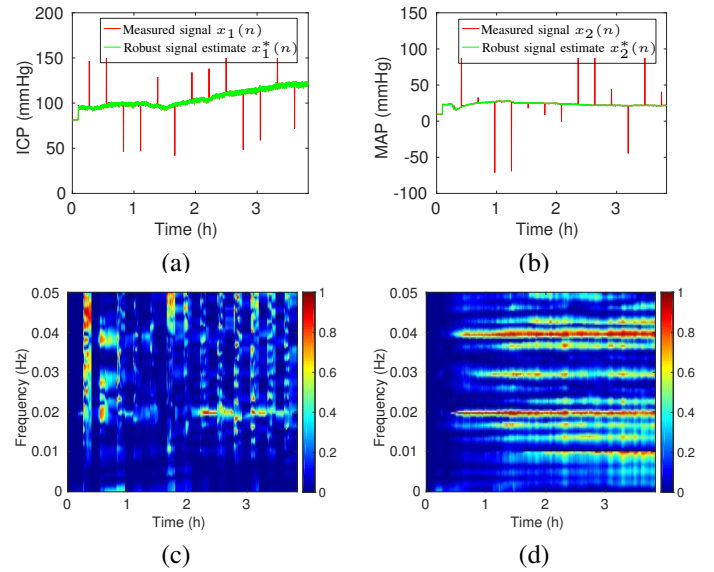(a)   (b)

(c)   (d)

Fig. 13. A simulation experiment to investigate the impact of artifacts on causality estimations and to evaluate the effectiveness of the proposed robust estimation method. In the experiment, we examined a 4 hours segment of (a) an ICP and (b) a MAP signal, where $x_1(n)$ and $x_2(n)$ are the measured signals, i.e. clean signals, on which artificial artifacts (sharp spikes) were added on a 15 minutes interval, and $x_1^*(n)$ and $x_2^*(n)$ are the robust signal estimates; (c) illustrates how introduced artifacts distort and destroy the patterns in the non-robustly estimated TV-gPDC spectrum; and (d) then demonstrates how the proposed method is robust against artifacts and able to reveal the causality patterns in the rTV-gPDC spectrum.

following parameters were chosen: $P_{\mathrm{opt}} = 35, Q_{\mathrm{opt}} = 2$ and $\lambda_{\mathrm{opt}} = 0.04$, see Fig. 11a and Fig. 11b.

A. Robustness Against Artifacts

Fig. 12 illustrates that ICP and MAP signals, given as measured signals $x_1(n)$ and $x_2(n)$ respectively, can often be contaminated with artifacts and outliers. Thus, the nonrobust estimation of TVAR and TVMA model parameters result in errors, whereas the use of robust signal estimates, $x_1^*(n)$ and $x_2^*(n)$, yield robust estimates of the parameters. Moreover, the artifacts in the measured signals also cause errors in the estimation of causality. To investigate the impact of artifacts on causality estimation and to evaluate the effectiveness of the proposed robust estimation method, a numerical experiment was conducted.

As shown in Fig. 13, artificial artifacts (sharp spikes highlighted in red) were added on a 15 minutes interval to a 4 hour segment of clean (a) ICP and (b) MAP signals. These introduced artifacts heavily distort the non-robustly estimated rTV-gPDC spectrum in Fig. 13c. Nevertheless, as demonstrated in Fig. 13d, the proposed robust method is able to smoothly estimate and reconstruct the patterns in the rTV-gPDC spectrum despite the presence of artifacts. This experiment justifies both the need and effectiveness of the proposed robust method for causality estimation.

B. Causality and Patient Outcome

Experiments were conducted to compare the robust time-varying generalized partial directed coherence (rTV-gPDC)

spectra of patients with good and poor outcome. Pairwise causality among ICP, MAP and PtiO2 patients were investigated. Outcomes of the patients were measured with the Glasgow Outcome Scale (GOS). Figures 14 and 15 showcase the rTV-gPDC spectra of patient A and B, who did not survive, and Fig. 16 shows the rTV-gPDC spectra of patient C, who achieved good recovery outcome. We observed that: for patients A and B, there was high connectivity between ICP $\rightarrow$ PtiO2 and MAP $\rightarrow$ PtiO2 in the frequency regions around 0.01 Hz; however, this connectivity does not exist in patient C. We suspect that strong causality observed in patient A and B may suggest ineffective autoregulations, which eventually lead to poor outcomes. Moreover, the detected oscillations around 0.01 Hz may also indicate the presence of a B-wave (around 0.5-2 cycle/minute [64]), which were found to indicate the failing intracranial compensation [65].

C. Linear and Nonlinear Causality

In current practices, cerebrovascular autoregulation is commonly assessed based on the pressure-reactivity index (PRx), which is defined as a sliding window linear correlation between the ICP and MAP signals. Our proposed method has the advantage that it enables the simultaneous monitoring of the linear and nonlinear causality between ICP and MAP. Fig. 17 shows two examples that compare the linear and nonlinear causality MAP $\rightarrow$ ICP. We observed that, over certain regions (e.g. second half of Fig. 17a and first half of Fig. 17b), the estimated linear and nonlinear causality align closely. At the same time, there are regions (first half of Fig. 17a and second half of Fig. 17b), where almost no linear causality
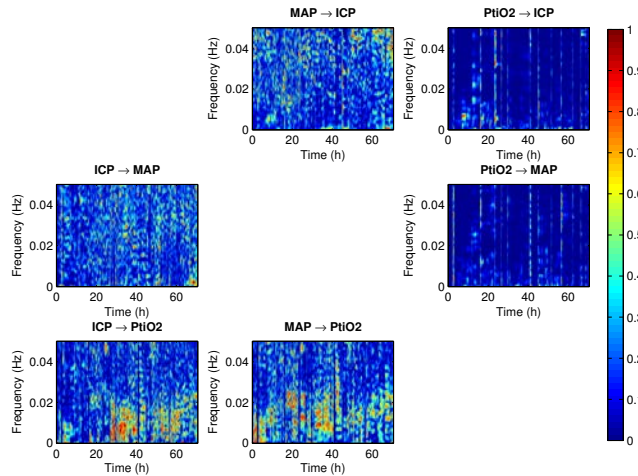
Fig. 14. Linear time-varying generalized partial directed coherence of ICP, MAP, and PtiO2 of patient A
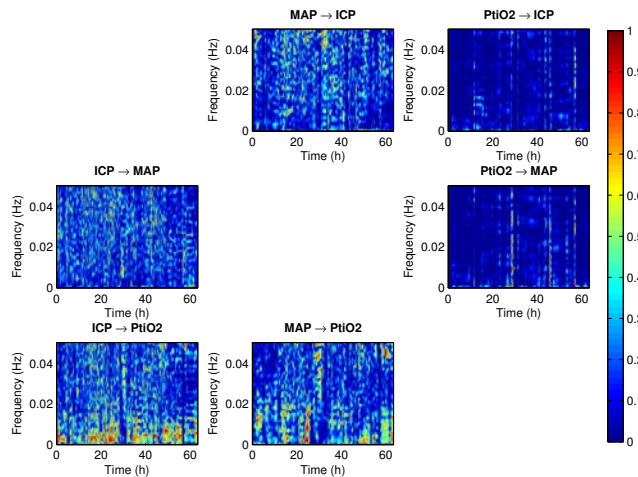

Fig. 15. Linear time-varying generalized partial directed coherence of ICP, MAP, and PtiO2 of patient B
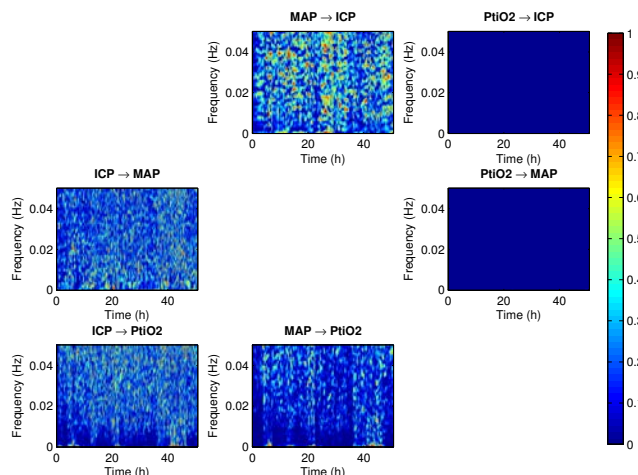

Fig. 16. Linear time-varying generalized partial directed coherence of ICP, MAP, and PtiO2 of patient C

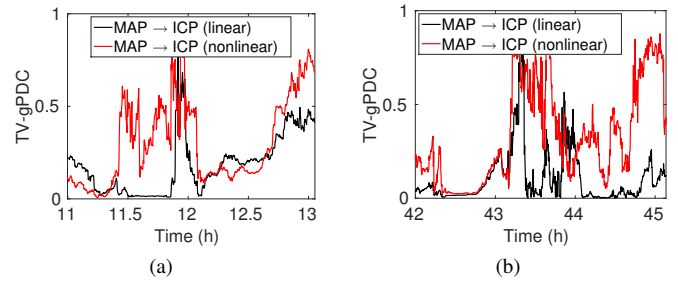Fig. 17. Two exemplary excerpts to compare the linear and nonlinear rTV-gPDC at a fixed frequency ($f = 0.0075$ Hz) from MAP $\rightarrow$ ICP.

existed but a significant nonlinear causality was observed. This suggests that there are nonlinear correlations between neurophysiological signals that will not be captured by any linear causality measure. Therefore, it may be worthwhile to further investigate how estimation of nonlinear causality may help to better measure cerebrovascular autoregulation.

VI. Discussion

This Section provides a brief discussion on a selection of parameters of the Kalman filter, as well as a description of the findings and limitations of the presented TBI study.

A. Discussion of the Method

The update coefficient λ plays a role in how fast the Kalman filter algorithm adapts to statistical changes of the signal, as it controls the memory of the adaptive algorithm. By increasing λ, the filter will adapt quicker to the signal and the general accuracy of the estimated signal is increased. On the other hand a small value of λ can increase robustness against long bursts of outliers.

Thus, the determination of λ is a trade-off between adaptation speed and robustness.

Another parameter to adjust the robustness of the Kalman filter is the length of the signal window L to estimate a robust mean in (32) and (31) and to estimate a robust standard deviation in (33) and (34). As longer windows incorporate more samples, the estimate improves for stationary (or very slowly varying) signals. For highly non-stationary signals, this parameter should not be too large, so that it captures the quickly varying temporary characteristics. In this work, the window length is chosen to be $L = \max(P, 50)$.

B. Findings and Limitations of the TBI Case Study

We observed that the proposed method is robust against artifacts and outliers in the TBI data and is capable to correct the influence from artifacts and reconstruct patterns in the causality spectrum. We also demonstrated that the proposed method can simultaneously capture linear and nonlinear causality between neurophysiological time series signals, which may offer additional information to allow better understanding of patients' cerebrovascular autoregulation status. Moreover, significant patterns were observed in the causality spectrum

that may act as new biomarkers to differentiate patients with good and poor outcomes.

A limitation of the case study is its small cohort size. Therefore, we did not aim to conclude any clinical findings through the study. The case study aimed at demonstrating the capabilities and limitations of the proposed method as a new and effective tool to explore causality spaces that were not studied before. Some interesting observations were discovered, which can inspire more comprehensive and systematic clinical studies for further investigations.

The Matlab implementation of the code for estimating the linear and nonlinear TV-gPDC functions can be requested from the first author.

VII. Conclusion

A new robust time-varying generalized partial directed coherence (rTV-gPDC) measure was proposed. Robustness against artifacts was incorporated via a computationally simple one-step reweighting step in a Kalman filter. The proposed method reveals nonlinear relations between multivariate time series by combination of a term that captures linear interactions and a second term that approximates the components that cannot be captured using a linear model. We evaluated our method numerically both in terms of accuracy and robustness and compared it to an existing method. We applied our method to real life multivariate time series from traumatic brain injuries patients to showcase its potential clinical applications. Since restrictive assumptions on the stationarity of the signals and the linearity of their relationship were relaxed, and robustness against artifacts incorporated via a computationally simple manner, the rTV-gPDC is potentially a good candidate to analyze a broad range of signals.

Acknowledgment

References

[1] J. P. Kaipio and P. A. Karjalainen, "Estimation of event-related synchronization changes by a new TVAR method," *IEEE Trans. Biomed. Eng.*, vol. 44, no. 8, pp. 649–656, Aug 1997.

[2] L. A. Baccalá *et al.*, "Studying the interaction between brain structures via directed coherence and Granger causality," *Appl. Signal Process.*, vol. 5, no. 1, pp. 40–48, 1998.

[3] J. R. Sato *et al.*, "Frequency domain connectivity identification: An application of partial directed coherence in fMRI," *Hum. Brain Mapp.*, vol. 30, no. 2, pp. 452–461, 2009.

[4] Z. G. Zhang *et al.*, "Local polynomial modeling of time-varying autoregressive models with application to time-frequency analysis of event-related EEG," *IEEE Trans. Biomed. Eng.*, vol. 58, no. 3, pp. 557–566, March 2011.

[5] G. Varotto *et al.*, "Enhanced frontocentral EEG connectivity in photosensitive generalized epilepsies: A partial directed coherence study," *Epilepsia*, vol. 53, no. 2, pp. 359–367, 2012.

[6] M. Orini *et al.*, "Assessment of the dynamic interactions between heart rate and arterial pressure by the cross time-frequency analysis," *Physiol. Meas.*, vol. 33, no. 3, pp. 315–331, 2012.

[7] ——, "A multivariate time-frequency method to characterize the influence of respiration over heart period and arterial pressure," *EURASIP J. Adv. Signal Process.*, vol. 2012, no. 1, pp. 1–17, 2012.

[8] M. D. Peláez-Coca *et al.*, "Cross time-frequency analysis for combining information of several sources: Application to estimation of spontaneous respiratory rate from photoplethysmography," *Comput. Math. Methods Med.*, vol. 2013, 2013.

[9] B. Boashash *et al.*, "Time-frequency processing of nonstationary signals: Advanced TFD design to aid diagnosis with highlights from medical applications," *IEEE Signal Process. Mag.*, vol. 30, no. 6, pp. 108–119, Nov 2013.

[10] Y. Höller *et al.*, "Connectivity biomarkers can differentiate patients with different levels of consciousness," *Clin. Neurophysiol.*, vol. 125, no. 8, pp. 1545–1555, 2014.

[11] L. Faes *et al.*, "Causal transfer function analysis to describe closed loop interactions between cardiovascular and cardiorespiratory variability signals," *Biol. Cybern.*, vol. 90, no. 6, pp. 390–399, 2004.

[12] ——, "Causal cross-spectral analysis of heart rate and blood pressure variability for describing the impairment of the cardiovascular control in neurally mediated syncope," *IEEE Trans. Biomed. Eng.*, vol. 53, no. 1, pp. 65–73, Jan. 2006.

[13] L. Faes and G. Nollo, "Extended causal modeling to assess partial directed coherence in multiple time series with significant instantaneous interactions," *Biol. Cybern.*, vol. 103, no. 5, pp. 387–400, 2010.

[14] L. Faes *et al.*, "Measuring connectivity in linear multivariate processes: Definitions, interpretation, and practical analysis," *Comput. Math. Methods Med.*, vol. 2012, p. 140513, 2012.

[15] M. Orini *et al.*, "Characterization of dynamic interactions between cardiovascular signals by time-frequency coherence," *IEEE Trans. Biomed. Eng.*, vol. 59, no. 3, pp. 663–673, 2012.

[16] G. C. Carter, "Coherence and time delay estimation," *Proc. IEEE*, vol. 75, no. 2, pp. 236–255, Feb. 1987.

[17] J. S. Bendat and A. G. Piersol, *Random data: Analysis and measurement procedures*. John Wiley & Sons, 2011, vol. 729.

[18] M. Muma *et al.*, "The role of cardiopulmonary signals in the dynamics of the eye's wavefront aberrations," *IEEE Trans. Biomed. Eng.*, vol. 57, no. 2, pp. 373–383, Feb. 2010.

[19] M. Kaminski and K. Blinowska, "A new method of the description of the information flow in the brain structures," *Biol. Cybern.*, vol. 65, no. 3, pp. 203–210, 1991.

[20] Y. Saito and H. Harashima, "Tracking of information within multichannel EEG record: Causal analysis in EEG," in *Recent Advances in EEG and EMG Data Processing*, N. Yamaguchi and K. Fujisawa, Eds. New York: Elsevier, 1981, pp. 133–146.

[21] L. A. Baccalá and K. Sameshima, "Partial directed coherence: A new concept in neural structure determination," *Biol. Cybern.*, vol. 84, no. 6, pp. 463–474, 2001.

[22] L. A. Baccalá *et al.*, "Generalized partial directed coherence," in *Proc. 15th Int. Conf. Digit. Signal Process.*, 2007, pp. 163–166.

[23] T. Milde *et al.*, "A new kalman filter approach for the estimation of high-dimensional time-variant multivariate AR models and its application in analysis of laser-evoked brain potentials," *Neuroimage*, vol. 50, no. 3, pp. 960 – 969, 2010.

[24] L. Leistritz *et al.*, "Time-variant partial directed coherence for analysing connectivity: A methodological study," *Phil. Trans. Roy. Soc. A*, vol. 371, no. 1997, 2013.

[25] L. A. Baccalá *et al.*, "Unified asymptotic theory for all partial directed coherence forms," *Phil. Trans. Roy. Soc. A*, vol. 371, no. 1997, 2013.

[26] A. Omidvarnia *et al.*, "Measuring time-varying information flow in scalp EEG signals: Orthogonalized partial directed coherence," *IEEE Trans. Biomed. Eng.*, vol. 61, no. 3, pp. 680–693, 2014.

[27] C. W. J. Granger, "Investigating causal relations by econometric models and cross-spectral methods," *Econometrica*, vol. 37, pp. 424–438, 1969.

[28] E. Möller *et al.*, "Fitting of one ARMA model to multiple trials increases the time resolution of instantaneous coherence," *Biol. Cybern.*, vol. 89, no. 4, pp. 303–312, 2003.

[29] G. A. Giannakakis and K. S. Nikita, "Estimation of time-varying causal connectivity on EEG signals with the use of adaptive autoregressive parameters," in *Proc. 30th Annu. Int. Conf. Eng. Med. Biol. Soc.*, 2008, pp. 3512–3515.

[30] S. Heritier *et al.*, *Robust Methods in Biostatistics*, D. J. Balding *et al.*, Eds. Wiley, 2009.

[31] P. van Mierlo *et al.*, "Accurate epileptogenic focus localization through time-variant functional connectivity analysis of intracranial electroencephalographic signals," *Neuroimage*, vol. 56, no. 3, pp. 1122–1133, 2011.

[32] L. Faes *et al.*, "Testing frequency domain causality in multivariate time series," *IEEE Trans. Biomed. Eng.*, vol. 57, no. 8, pp. 1897–1906, Aug. 2010.

[33] N. Nicolaou *et al.*, "EEG-based automatic classification of 'awake' versus 'anesthetized' state in general anesthesia using Granger causality," *PLoS ONE*, vol. 7, no. 3, p. e33869, Mar. 2012.

[34] A. M. Zoubir *et al.*, "Robust estimation in signal processing: A tutorial-style treatment of fundamental concepts," *IEEE Signal Process. Mag.*, vol. 29, no. 4, pp. 61–80, 2012.

[35] F. Strasser *et al.*, "Motion artifact removal in ECG signals using multi-resolution thresholding," in *Proc. 20th European Signal Process. Conf.*, 2012, pp. 899–903.

[36] S. L. Bressler and A. K. Seth, "Wiener–Granger causality: A well established methodology," *Neuroimage*, vol. 58, no. 2, pp. 323–329, 2011.

[37] E. Pereda *et al.*, "Nonlinear multivariate analysis of neurophysiological signals," *Progr. Neurobiol.*, vol. 77, no. 1, pp. 1–37, 2005.

[38] D. Marinazzo *et al.*, "Nonlinear connectivity by Granger causality," *Neuroimage*, vol. 58, no. 2, pp. 330–338, 2011.

[39] F. He *et al.*, "A nonlinear causality measure in the frequency domain: Nonlinear partial directed coherence with applications to EEG," *J. Neurosci. Methods*, vol. 225, pp. 71 – 80, 2014.

[40] P. J. Huber and E. Ronchetti, *Robust Statistics*, 2nd ed. New York, NY, USA: Wiley, 2009.

[41] R. A. Maronna *et al.*, *Robust Statistics: Theory and Methods*, ser. Wiley Series in Probability and Statistics. Hoboken, NJ: Wiley, 2006.

[42] F. Chowdhury, "Input-output modeling of nonlinear systems with time-varying linear models," *IEEE Trans. Autom. Control*, vol. 45, no. 7, pp. 1355–1358, Jul. 2000.

[43] A. Omidvarnia *et al.*, "Kalman filter-based time-varying cortical connectivity analysis of newborn EEG," in *Proc. 33th Annu. Int. Conf. Eng. Med. Biol. Soc.*, 2011, pp. 1423–1426.

[44] C. W. J. Granger, "Testing for causality: A personal viewpoint," *J. Econ. Dyn. Control*, vol. 2, pp. 329–352, 1980.

[45] W. Hesse *et al.*, "The use of time-variant EEG granger causality for inspecting directed interdependencies of neural assemblies," *J. Neurosci. Methods*, vol. 124, pp. 27–44, 2003.

[46] Y. Li *et al.*, "Time-varying linear and nonlinear parametric model for Granger causality analysis," *Phys. Rev. E*, vol. 85, no. 4, p. 041906, Apr. 2012.

[47] Y. Liu and M. T. Bahadori, "A survey on Granger causality: A computational view," *University of Southern California*, pp. 1–13, 2012.

[48] A. M. Zoubir and B. Boashash, "The bootstrap and its application in signal processing," *IEEE Signal Process. Mag.*, vol. 15, no. 1, pp. 56–76, Jan 1998.

[49] A. M. Zoubir and D. R. Iskander, *Bootstrap techniques for signal processing*. Cambridge University Press, 2004.

[50] D. J. Simon, "Using nonlinear Kalman filtering to estimate signals," *Embedded Syst. Des.*, vol. 19, no. 7, pp. 38–53, Jul. 2006.

[51] R. B. Buxton *et al.*, "Modeling the hemodynamic response to brain activation," *Neuroimage*, vol. 23, no. Suppl 1, pp. S220–S233, 2004.

[52] M. Czosnyka and J. D. Pickard, "Monitoring and interpretation of intracranial pressure," *J. Neurol. Neurosurgery Psych.*, vol. 75, no. 5, pp. 813–821, Jun. 2004.

[53] E. Möller *et al.*, "Instantaneous multivariate EEG coherence analysis by means of adaptive high-dimensional autoregressive models," *J. Neurosci. Methods*, vol. 105, pp. 143–158, 2001.

[54] M. Havlicek *et al.*, "Dynamic Granger causality based on Kalman filter for evaluation of functional network connectivity in fMRI data," *Neuroimage*, vol. 53, no. 1, pp. 65–77, 2010.

[55] L. Sommerlade *et al.*, "Time-variant estimation of directed influences during Parkinsonian tremor," *J. Physiol. Paris*, vol. 103, no. 6, pp. 348–352, 2009.

[56] M. Kamiński *et al.*, "Evaluating causal relations in neural systems: Granger causality, directed transfer function and statistical assessment of significance," *Biol. Cybern.*, vol. 85, no. 2, pp. 145–157, 2001.

[57] C. Werner and K. Engelhard, "Pathophysiology of traumatic brain injury," *Br. J. Anaesth.*, vol. 99, no. 1, pp. 4–9, 2007.

[58] R. Hlatky *et al.*, "Intracranial pressure response to induced hypertension: Role of dynamic pressure autoregulation," *Neurosurgery*, vol. 57, no. 5, pp. 917–923, 2005.

[59] M. Czosnyka *et al.*, "Continuous assessment of the cerebral vasomotor reactivity in head injury." *Neurosurgery*, vol. 41, no. 1, pp. 11–17, 1997.

[60] A. Marmarou *et al.*, "A nonlinear analysis of the cerebrospinal fluid system and intracranial pressure dynamics," *J. Neurosurgery*, vol. 48, no. 3, pp. 332–344, 1978.

[61] M. Feng *et al.*, "Artifact removal for intracranial pressure monitoring signals: A robust solution with signal decomposition," in *Proc. 33th Annu. Int. Conf. Eng. Med. Biol. Soc.*, 2011, pp. 797–801.

[62] B. Han *et al.*, "An online approach for intracranial pressure forecasting based on signal decomposition and robust statistics," in *Proc. Int. Conf. Acoust., Speech, Signal Process.*, 2013, pp. 6239–6243.

[63] H. Akaike, "A new look at the statistical model identification," *IEEE Trans. Autom. Control*, vol. 19, no. 6, pp. 716–723, Dec 1974.

[64] J. Krauss *et al.*, "The relation of intracranial pressure b-waves to different sleep stages in patients with suspected normal pressure hydrocephalus," *Acta Neurochirurgica*, vol. 136, no. 3-4, pp. 195–203, 1995.

[65] L. Auer and I. Sayama, "Intracranial pressure oscillations (b-waves) caused by oscillations in cerebrovascular volume," *Acta Neurochirurgica*, vol. 68, no. 1-2, pp. 93–100, 1983.

Tim Schäck (S'13) received the Dipl.-Ing. degree in Electrical Engineering and Information Technology from Technische Universität Darmstadt, Darmstadt, Germany, in 2013.

He is currently working toward the Ph.D. degree in the Signal Processing Group, Institute of Telecommunications, Technische Universität Darmstadt, Darmstadt, Germany. His research focuses on biomedical signal processing. He was the supervisor of the Technische Universität Darmstadt student team who won the international IEEE Signal Processing Cup 2015, the competition topic was "Heart Rate Monitoring During Physical Exercise Using Wrist-Type Photoplethysmographic (PPG) Signals".

Michael Muma (S'10–M'14) received the Dipl.-Ing (2009) and the Ph.D. (Dr.-Ing.) degree with summa cum laude in Electrical Engineering and Information Technology (2014), both from Technische Universität Darmstadt, Darmstadt, Germany. He completed his diploma thesis with the Contact Lens and Visual Optics Laboratory, School of Optometry, Brisbane, Australia, on the role of cardiopulmonary signals in the dynamics of the eye's wavefront aberrations. His PhD thesis was on "Robust Estimation and Model Order Selection for Signal Processing".

Currently, he is a Postdoctoral Fellow at the Signal Processing Group, Institute of Telecommunications, Technische Universität Darmstadt. His research is on robust statistics for signal processing, biomedical signal processing, and robust distributed detection, classification and estimation for wireless sensor networks.

Dr. Muma has been the IEEE SPS Signal Processing Theory and Methods Student Subcommittee Chair since 2011. He organized a Special Session on "Advances in Robust Statistical Signal Processing" at the 2014 IEEE Workshop on Statistical Signal Processing (SSP) at Jupiters, Gold Coast, Australia held from 29 June to 2 July 2014. Since 2015, he is an Associate Editor for the IEEE Signal Processing eNewsletter representing the Europe region. Dr. Muma was the supervisor of the Technische Universität Darmstadt student team who won the international IEEE Signal Processing Cup 2015, the competition topic was "Heart Rate Monitoring During Physical Exercise Using Wrist-Type Photoplethysmographic (PPG) Signals".

Mengling Feng is currently an Assistant Professor in both the Saw Swee Hock School of Public Health and Yong Loo Lin School of Medicine, National University of Singapore. Dr. Feng is also an affiliated scientist with the Lab of Computational Physiology, Harvard-MIT Health Science Technology Division. His research is to develop effective medical Big Data management and analysis methods to extract actionable knowledge to improve the quality of care. His research brings together concepts and tools across machine learning, optimization, signal processing, statistical causal inference and big data management. In particular, he has been publishing on physiological signal forecasting, modeling of disease progress trajectory, dynamic patient phenotyping, statistical understanding of treatment effects and management of heterogeneous medical big data. Dr. Feng works closely with clinicians around the world, and he also collaborates with major healthcare and IT companies, such as Philips and SAP. Dr. Feng's work was recognized by both well-established journals and top conferences, such as Science Translational Medicine, IEEE Journal of Biomedical and Health Informatics, KDD, AAAI and AMIA.

Abdelhak M. Zoubir (S'87–M'92–SM'97–F'08) received his Dr.-Ing. from Ruhr-Universit?t Bochum, Germany, in 1992. He was with Queensland University of Technology, Australia, from 1992–1998, where he was Associate Professor. In 1999, he joined Curtin University of Technology, Australia, as a Professor of Telecommunications and was Interim Head of the School of Electrical & Computer Engineering from 2001 until 2003. In 2003, he moved to Technische Universität Darmstadt, Germany, as Professor of Signal Processing and Head of the Signal Processing Group. His research interest lies in statistical methods for signal processing with emphasis on bootstrap techniques, robust detection and estimation and array processing applied to telecommunications, radar, sonar, automotive monitoring and safety, and biomedicine. He published over 400 journal and conference papers on these areas. Professor Zoubir was General or Technical Co-Chair of numerous conferences and workshops, more recently, he was the Technical Co-Chair of ICASSP-14. He also served on various editorial boards and more recently, he was the Editor-In-Chief of the IEEE Signal Processing Magazine (2012–2014). Dr. Zoubir was Past Chair (2012), Chair (2010–2011), Vice-Chair (2008–2009) and Member (2002–2007) of the IEEE SPS Technical Committee Signal Processing Theory and Methods (SPTM). He was a Member of the IEEE SPS Technical Committee Sensor Array and Multi-channel Signal Processing (SAM) from 2007 until 2012. He also serves on the Board of Directors of the European Association of Signal Processing (EURASIP) and is an elected member of the IEEE SPS Board of Governors. He is an IEEE Distinguished Lecturer (Class 2010–2011).

Cuntai Guan (S'91–M'92–SM'03) is currently Principal Scientist and Department Head at the Institute for Infocomm Research, Agency for Science, Technology and Research (A*STAR), Singapore. He is the A*STAR MedTech Programme Leader of Neuro-Technology. He is co-Director of Rehabilitation Research Institute of Singapore. He is also a full Professor with the School of Computer Engineering, Nanyang Technological Univeristy (NTU). Since 2003, he founded and directed the Brain-computer Interface (BCI) Laboratory at the Institute for Infocomm Research (http://nsp.i2r.a-star.edu.sg/). From 2007 to 2012, he founded and directed two research programs on medical and healthcare technology at the Institute for Infocomm Research. Since 2012, he founded and directed a research department, Neural & Biomedical Technology Department at the Institute for Infocomm Research. He initiated and co-established the Rehabilitation Research Institute of Singapore (RRIS), an $100M initiative by A*STAR, NTU and National Health Group. His research interests include neural and biomedical signal processing, machine learning and pattern recognition, neural and cognitive process and its clinical applications, brain?computer interface algorithms, systems and applications, statistical signal processing, neural image processing, medical system and device research and development. He is the recipient of Annual BCI Research Award, IES Prestigious Engineering Achievement Award, Achiever of the Year (Research) Award, etc. He published over 250 refereed journal and conference papers and holds 18 granted patents and applications. He licensed 8 patents to US and Singapore based companies. He secured over $17M research grant as principal investigator and co-investigator since 2009. He delivered over 50 keynote speech and invited talks. He is an Associate Editor of IEEE Transactions on Biomedical Engineering, IEEE Access (life sciences and biomedical engineering), Frontiers in Neuroprosthetics, Brain Computer Interfaces, A*STAR Research Publication, and Guest-Editor for IEEE Computational Intelligence Magazine.